

# Unsteady aerodynamics of porous aerofoils

Peter J. Baddoo<sup>1</sup>, Rozhin Hajian<sup>2</sup>, and Justin W. Jaworski<sup>3</sup>

<sup>1</sup>Department of Applied Mathematics and Theoretical Physics, University of Cambridge, Cambridge, CB3 0WA, United Kingdom

<sup>2</sup>School of Engineering and Applied Sciences, Harvard University, Cambridge, Massachusetts 02138

<sup>3</sup>Department of Mechanical Engineering and Mechanics, Lehigh University, Bethlehem, Pennsylvania 18015

(Received xx; revised xx; accepted xx)

We extend unsteady thin aerofoil theory to model aerofoils with generalized chordwise porosity distributions. The analysis considers a Darcy-type porosity law where the seepage velocity through the aerofoil is linearly related to the local pressure jump across the aerofoil surface. Application of the Plemelj formulae yields a singular Fredholm–Volterra integral equation which does not admit an analytic solution. Accordingly, we develop a numerical solution scheme by expanding the bound vorticity distribution in terms of appropriate basis functions. Asymptotic analysis at the leading- and trailing-edges reveals that the appropriate basis functions are weighted Jacobi polynomials whose parameters are related to the porosity distribution. The Jacobi polynomial basis enables the construction of a numerical scheme that is accurate and rapid, in contrast to the standard choice of Chebyshev basis functions that are shown to be ill-posed in their application to porous aerofoils. The numerical scheme is demonstrated to remain valid when the porosity gradient has an interior discontinuity. Porous analogues to the classical Theodorsen and Sears functions are computed numerically, which show that an effect of trailing-edge porosity is to reduce the amount of vorticity shed into the wake, thereby reducing the magnitude of the circulatory lift. Results from the present analysis and its underpinning numerical framework aim to enable the unsteady aerodynamic assessment of design strategies using porosity, which has implications for noise-reducing aerofoil design and biologically-inspired flight.

**Key words:** aerodynamics, aeroacoustics, flow-structure interaction

---

## 1. Introduction

The seminal works of Theodorsen (1935) and Sears (1941) continue to ground the modern understanding of unsteady aerodynamic phenomena experienced by lifting bodies. Their analyses considered the unsteady potential flow about an impermeable aerofoil: whilst Theodorsen considered the effect of unsteady (harmonic) aerofoil motions, Sears was concerned with the fluctuating pressure response of the aerofoil to an incident harmonic gust. Both authors were able to derive closed-form, analytic expressions for the unsteady lift in terms of Hankel functions, whose use is now widespread in aerodynamic studies. The analysis of Theodorsen was originally motivated by the need to predict flutter instability but has been used *inter alia* to form the basis for predicting and comparing unsteady forces on flapping foils (Garrick 1936; Jaworski & Gordnier 2012, 2015; Floryan

*et al.* 2017) and to develop load prediction methods relevant to rotorcraft blades (Loewy 1957; Peters 2008). The work of Sears relates directly to aerodynamic gust responses and enables the prediction of acoustic radiation from aerofoils encountering vortical sources (see Glegg & Devenport 2017), where extensions to Sears’s analysis have included the distortion of the incoming gust by the aerofoil (Goldstein & Atassi 1976), as well as the effects of mean aerofoil loading (Scott & Atassi 1993), aerofoil shape (Kerschen *et al.* 1993), and finite Mach number (Graham 1970).

Understanding, exploiting, and extending the analyses of Theodorsen and Sears remains a vibrant area of research. Recent work by Cordes *et al.* (2017) explored the limitations of the transfer functions and found that, whilst the Theodorsen function performed well against experimental data, the Sears function required the second-order correction for gust distortion by the aerofoil provided by Goldstein & Atassi (1976) and Atassi (1984). The discrepancies between these models were investigated in greater detail by Wei *et al.* (2019), who concluded that the original Sears function may even be used when there are considerable fluctuations in the streamwise velocity component. Of particular note is the recent extension of unsteady potential flow to include viscosity via triple deck analysis at the trailing edge by Taha & Rezaei (2019). In particular, this work presented a viscous extension of the Theodorsen function to elucidate the role of viscosity-induced lag that becomes increasingly important at large reduced frequencies. Extension of the transfer functions from two-dimensional aerofoils to three-dimensional wings is another popular research direction, which has been pursued with a variety of possible methods (Bird *et al.* 2019; Yang *et al.* 2019). However, the original analyses by Theodorsen and Sears and these subsequent investigations they have inspired involve impermeable lifting surfaces that do not permit any flow seepage through the aerofoil or wing. In the present work, we extend these classical unsteady analyses to consider aerofoils with chordwise porosity gradients. In particular, we consider a Darcy porosity law where the seepage velocity is linearly proportional to the local pressure gradient across the aerofoil.

Porous aerofoils have received considerable attention over recent years due to their apparent ability to reduce acoustic emissions (Geyer *et al.* 2010; Jaworski & Peake 2013; Ayton 2016; Kisil & Ayton 2018). It is generally believed that porosity at the trailing edge weakens the scattering of turbulence there and therefore reduces sound production in a manner similar to turbulence noise suppression by an edgeless perforated sheet (Ffowcs Williams 1972; Nelson 1982). However, the fluid loads on perforated aerofoils are also affected by porosity and are expected to be aerodynamically poorer in comparison to impermeable aerofoils (Geyer *et al.* 2010; Iosilevskii 2011, 2013; Hajian & Jaworski 2017). Recent experiments by Hanna & Spedding (2019) demonstrate that porosity can also be aerodynamically beneficial by suppressing unwanted flow phenomena that are dependent upon the Reynolds number of the configuration. Consequently, aircraft designers seeking to use porosity as a noise mitigation strategy are faced with the difficult task of balancing the aeroacoustic advantages of porous aerofoils with their aerodynamic disadvantages.

With the goal to assess these aerodynamic effects, Hajian & Jaworski (2017) developed an analytic formulation and solution for the steady aerodynamic loads on airfoils with arbitrary, realistic (specifically, Hölder continuous) porosity distributions to investigate the impact of a chordwise variation in porosity. This analysis was later extended to determine the unsteady forces on an arbitrarily deforming panel with generalized porosity distributions (Hajian & Jaworski 2019). An analytical expression for the unsteady pressure distribution was presented and evaluated for the special cases of uniform and variable-porosity panels undergoing harmonic deformations, where the effect of the panel end conditions was also investigated.

A comprehensive unsteady aerodynamic theory for lifting porous bodies is also essential to predict aeroelastic stability and aeroacoustic emissions. The classical theory of Theodorsen (1935) and its later extensions (Jaworski 2012) developed closed-form expressions for the unsteady aerodynamic forces on a piecewise-continuous impermeable airfoil undergoing small-amplitude harmonic motions in a uniform incompressible flow. These analyses separated the total fluid forces or moments into circulatory and non-circulatory parts, which correspond respectively to the contribution of the unsteady shedding of vorticity into the wake and the non-lifting hydrodynamic reaction of fluid to aerofoil motion. These unsteady fluid forces also contribute fundamentally to the aerofoil gust response problem (cf. Bisplinghoff *et al.* 1996, pp. 281-293) and to the aerodynamic noise generation from gust encounters (Atassi *et al.* 1993) and vortex-structure interactions (Howe 2002). Therefore, an extension of the classical unsteady aerodynamic response models to include the effects of porosity distributions is desired.

The classical aerodynamic functions for impermeable aerofoils depend on the solution of a singular integral equation for the vorticity or pressure distribution on the aerofoil, which may be integrated to furnish the aerodynamic loads of interest. Schwarz (1940) employed the integral inversion of Söhngen (1939) to produce an exact solution for the pressure distribution and fluid loads on unsteady impermeable aerofoils. Hajian & Jaworski (2017) determined an exact solution for steady aerofoils with chordwise porosity gradients using conventional analysis methods (see Muskhelishvili 1946), as noted above. However, the singular integral equation describing the generalized aerodynamics of unsteady porous airfoils with a wake cannot be treated by conventional analysis, and a different mathematical approach is required. A new approach to circumvent the analytical challenges of unsteady porous aerofoil modelling is the focus of the present research.

In complement to standard analytical approaches, there are many methods available for the numerical solution of singular integral equations (Erdogan *et al.* 1973). Numerical solutions in terms of orthogonal polynomials were first considered by Erdogan & Gupta (1972), who expressed the solution function as a series of weighted Chebyshev polynomials. However, this numerical approach was limited to particular endpoint behaviours until the generalisation by Krenk (1975) to Jacobi polynomials allowed a broader class of endpoint zeros and singularities to be examined. In the present research, we adapt the approach of Krenk (1975) to a broader class of singular integral equations, including the generalisation to discontinuous coefficients.

The expansion of the jump in surface pressure across the aerofoil into a series of weighted Chebyshev polynomials has also been applied to aerodynamic problems for impermeable (Rienstra 1992) and permeable (Weidenfeld & Manela 2016) aerofoils. The weighted Chebyshev expansion (also referred to as a Glauert-Fourier series) is an essential feature of many reduced-order discrete-vortex models (Ramesh *et al.* 2014; SureshBabu *et al.* 2019). These models require detailed understanding of the pressure at the leading and trailing edges to predict the vortex shedding behaviour correctly. In particular, the leading-edge suction parameter must be accurately computed (Ramesh *et al.* 2014). In the present work, we show that the Chebyshev expansion is ill-posed for porous aerofoils, and an expansion in terms of weighted Jacobi polynomials is essential to capture the subtle behaviour at the endpoints.

The remainder of this paper is structured in the following manner. Section 2 presents the mathematical model for a porous wing undergoing unsteady motions, and a numerical solution of the ensuing singular integral equation is presented in §3. This numerical solution is then used to draw physical insights from a range of practical scenarios in §4. In particular, we develop porous analogues of the Theodorsen and Sears functions that

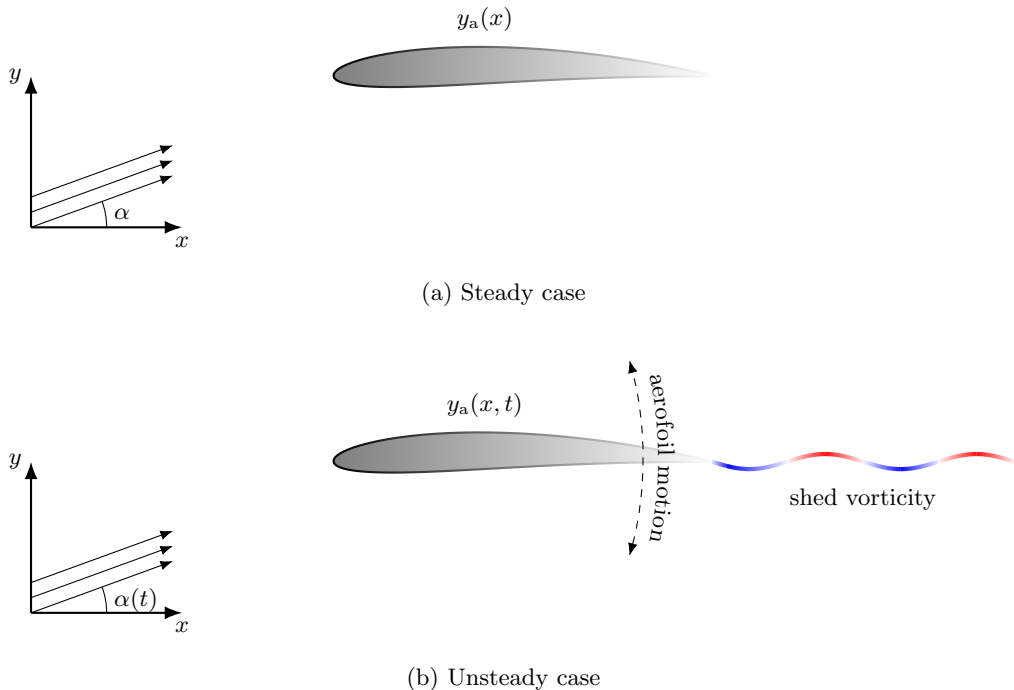


Figure 1: Schematic diagrams of a porous aerofoil with mean camber profile  $y_a$  at angle of attack  $\alpha$  for (a) steady and (b) unsteady scenarios. Aerofoil porosity is illustrated by the colour gradient on the aerofoils. In the unsteady case, the angle of attack and aerofoil surface profile may vary with time. A pitching motion is illustrated as an example, and the unsteady wake shed from the trailing edge is illustrated by the wavy line in (b).

must be computed numerically. Finally, §5 summarises the main findings of the research and outlines a number of possible directions of future work.

## 2. Mathematical model

We consider a thin airfoil embedded in a uniform, two-dimensional incompressible flow. In the steady case, the aerofoil and incident flow are stationary, whereas in the unsteady case the aerofoil and incident flow may be time-dependent as illustrated in figure 1. In the latter case, the aerofoil sheds vorticity into a wake whose strength is unknown. Supposing a semi-chord length  $l$ , mean flow speed  $U$ , and fluid density  $\rho$ , all terms are nondimensionalized using  $l$ ,  $l/U$ , and  $\frac{1}{2}\rho U^2$  as the length, time, and pressure scales, respectively.

Under the further assumption that the flow is irrotational away from the aerofoil and the wake, we may describe the flow completely in terms of a complex potential function,  $\phi$ . Furthermore, the Biot–Savart law enables the complex velocity to be expressed in the form

$$u(z, t) - iw(z, t) = \frac{1}{2\pi i} \int_{-1}^1 \frac{\gamma_a(\xi, t)}{\xi - z} d\xi + \frac{1}{2\pi i} \int_1^\infty \frac{\gamma_w(\xi, t)}{\xi - z} d\xi, \quad (2.1)$$

where  $z = x + iy$ , while  $\gamma_a$  and  $\gamma_w$  represent distributions of vorticity along the aerofoil chord and wake respectively. The functions  $\gamma_a$  and  $\gamma_w$  are unknown and must be determined subject to the aerofoil boundary conditions and the Kutta condition, which imposes a zero pressure jump at the trailing edge at all times.

### 2.1. Porous boundary condition

Along a porous airfoil, the perturbation flow velocity on the wing surface,  $w$ , is related to the local seepage flow rate directed along the unit normal to the panel surface,  $w_s$ , by

$$w(x, t) = w_s(x, t) + \frac{\partial y_a}{\partial x}(x, t) + \frac{\partial y_a}{\partial t}(x, t), \quad (2.2)$$

where the function  $y_a(x, t)$  defines the mean surface of the airfoil.

For an aerofoil with a Darcy-type porosity distribution under conditions that permit the omission of nonlinear flow and acoustic effects (cf. Nayfeh *et al.* 1975; Bauer 1977; Jordan 2005), the local flow rate is linearly proportional to the porosity and the pressure distribution across the porous medium (Lifanov *et al.* 1992; Hajian & Jaworski 2017):

$$w_s = \frac{1}{2} \delta R(x) \Delta p(x, t). \quad (2.3)$$

Here,  $\delta = \rho UC$  is the dimensionless porosity parameter (Hajian & Jaworski 2017), where  $C$  is the porosity coefficient,  $R(x)$  is a dimensionless function defining the porosity distribution, and  $\Delta p(x, t)$  is the dimensionless pressure jump (lower minus upper) across the airfoil. Comparison of the relationship between the local pressure jump  $\Delta p$  and seepage velocity  $w_s$  against the standard Darcy boundary condition (Bird *et al.* 1960, pp. 149-150) allows the product  $CR(x)$  to be defined in terms of physical parameters:

$$CR(x) = \frac{\kappa}{\mu d}. \quad (2.4)$$

The symbol  $\mu$  denotes the fluid viscosity,  $\kappa$  and  $d$  represent the permeability, and thickness of the porous material, respectively, all of which may vary with chordwise location  $x$ .

The linearised Bernoulli equation for unsteady flow enables the pressure to be expressed as a function of the velocity potential  $\phi$  as

$$p(x, y, t) = - \left( \frac{\partial \phi}{\partial x} + \frac{\partial \phi}{\partial t} \right). \quad (2.5)$$

Applying (2.5) to  $y = 0^\pm$ ,  $x > -1$ , and taking the difference from the upper and lower sides yields an expression for the pressure jump along the airfoil and the shed wake as

$$\Delta p(x, t) = -2 \left( \gamma_a(x, t) + \frac{\partial}{\partial t} \int_{-1}^x \gamma_a(\xi, t) d\xi \right), \quad -1 < x < 1, \quad (2.6.a)$$

$$\Delta p(x, t) = -2 \left( \gamma_w(x, t) + \frac{\partial}{\partial t} \int_1^x \gamma_w(\xi, t) d\xi + \frac{d\Gamma}{dt}(t) \right), \quad 1 < x, \quad (2.6.b)$$

where  $\Gamma$  represents the circulation around the aerofoil. Substitution of (2.6.a) into (2.3) enables the Darcy law (2.3) to be written as

$$w_s(x) = -\delta R(x) \left( \gamma_a(x, t) + \frac{\partial}{\partial t} \int_{-1}^x \gamma_a(\xi, t) d\xi \right). \quad (2.7)$$

On the other hand, application of the Plemelj formula (Ablowitz & Fokas 2003) to the Biot–Savart law (2.1) shows that the velocity on the wing  $w$  is related the vorticity

distributions on the aerofoil ( $\gamma_a$ ) and on the wake ( $\gamma_w$ ) through the following singular integral equation (Bisplinghoff *et al.* 1996, (5-313a)):

$$w(x, t) = \frac{1}{2\pi} \int_{-1}^1 \frac{\gamma_a(\xi, t)}{\xi - x} d\xi + \frac{1}{2\pi} \int_1^\infty \frac{\gamma_w(\xi, t)}{\xi - x} d\xi, \quad -1 < x < 1. \quad (2.8)$$

Substitution of (2.7) and (2.8) into (2.2) furnishes the integral equation

$$\begin{aligned} \psi(x) \left[ \gamma_a(x, t) + \frac{\partial}{\partial t} \int_{-1}^x \gamma_a(\xi, t) d\xi \right] \\ - \frac{1}{\pi} \int_{-1}^1 \frac{\gamma_a(\xi, t)}{\xi - x} d\xi - \frac{1}{\pi} \int_1^\infty \frac{\gamma_w(\xi, t)}{\xi - x} d\xi = -2 \left( \frac{\partial y_a}{\partial t} + \frac{\partial y_a}{\partial x} \right), \end{aligned} \quad (2.9)$$

for  $-1 < x < 1$ , where we have written  $\psi(x) = 2\delta R(x)$ .

We further assume harmonic motions of (non-dimensional) reduced frequency  $k$ , so that we may write the vorticity distributions and mean camber line as

$$\gamma_a(x, t) = \hat{\gamma}_a(x) e^{ikt}, \quad \gamma_w(x, t) = \hat{\gamma}_w(x) e^{ikt}, \quad \text{and} \quad y_a(x, t) = \hat{y}_a(x) e^{ikt}.$$

Since we do not allow any pressure jump across the wake, we require the bracketed term in (2.6.b) to vanish. Solving the associated integral equation yields

$$\hat{\gamma}_w(x) = -ik e^{ik(1-x)} \int_{-1}^1 \hat{\gamma}_a(\xi) d\xi = -ik \hat{\Omega} e^{-ikx}, \quad (2.10)$$

where we have also applied Kelvin's circulation theorem to enforce that the net circulation vanishes. We define the reduced circulation as  $\hat{\Omega} = e^{ik} \hat{\Gamma}$  where  $\hat{\Gamma}$  is the circulation around the aerofoil with the time dependence factored out. We also enforce the Kutta condition, namely that the pressure jump vanishes at the trailing-edge:

$$\Delta p(1) = 0.$$

Substitution of (2.10) into (2.9) yields

$$\mathcal{L}[\hat{\gamma}_a](x) = f_a(x) + \hat{\Omega} f_w(x) \quad (2.11)$$

for  $-1 < x < 1$ , where we use the notation  $\mathcal{L}$  to represent the operator

$$\mathcal{L}[f](x) \equiv ik\psi(x) \int_{-1}^x f(\xi) d\xi + \psi(x)f(x) - \frac{1}{\pi} \int_{-1}^1 \frac{f(\xi)}{\xi - x} d\xi. \quad (2.12)$$

The forcing functions  $f_a$  and  $f_w$  are defined as

$$f_a(x) = -2 \left( \frac{d\hat{y}_a}{dx}(x) + ik\hat{y}_a(x) \right), \quad (2.13)$$

$$f_w(x) = \frac{ik}{\pi} \int_1^\infty \frac{e^{-ik\xi}}{\xi - x} d\xi. \quad (2.14)$$

The subscript notation  $a$  and  $w$  is again employed here to symbolise that  $f_a$  corresponds to contributions from the mean aerofoil profile and its motions, whereas  $f_w$  corresponds to contributions from the unsteady wake. The problem is now to determine two quantities: the function  $\hat{\gamma}_a$  and the constant  $\hat{\Omega}$ .

The operator  $\mathcal{L}$  consists of two parts: a Volterra part (the first term in (2.12)), and a singular Fredholm integral part (the second and third terms in (2.12)). Accordingly, we refer to  $\mathcal{L}$  as a singular Fredholm–Volterra integral equation (SF–VIE). The literature on these types of integral equations is apparently non-existent: the closest comparisons that

could be found (Darwish 1999; Abdou 2003) considered only the case where the kernel is weakly singular and not the Cauchy principal value considered in the present work. In particular, it is the presence of the Volterra part of  $\mathcal{L}$  that precludes the possibility of a solution using the classical singular integral equations methods of Muskhelishvili (1946). Accordingly, we now seek a numerical solution by expanding  $\hat{\gamma}_a$  into an appropriate series of basis functions.

### 3. Numerical solution

We now introduce our numerical solution for the SF-VIE integral equation (2.11) that is central to the unsteady aerodynamics of porous aerofoils. We motivate our approach to the unsteady problem by first examining a numerical solution for the steady case.

#### 3.1. Motivation – the steady case

We first consider the case where the field is steady, as illustrated in figure 2a. The wake vanishes, and the SF-VIE (2.11) for the bound vorticity distribution becomes

$$\psi(x)\hat{\gamma}_a(x) - \frac{1}{\pi} \int_{-1}^1 \frac{\hat{\gamma}_a(\xi)}{\xi - x} d\xi = -2 \frac{d\hat{y}_a}{dx}(x), \quad -1 < x < 1. \quad (3.1)$$

In the impermeable case ( $\psi \equiv 0$ ), the typical approach is to expand  $\hat{\gamma}_a$  in terms of weighted Chebyshev polynomials (Rienstra 1992). However, this approach assumes behaviour of the vorticity at the endpoints of the chord. In particular, the vorticity distribution is usually written as

$$\hat{\gamma}_a(x) = \hat{\gamma}_0 \sqrt{\frac{1-x}{1+x}} + \sqrt{1-x^2} \sum_{n=1}^{\infty} \hat{\gamma}_n U_{n-1}(x), \quad (3.2)$$

where  $U_n$  are the Chebyshev polynomials of the second kind and  $\hat{\gamma}_n$  are coefficients to be determined. Consequently,  $\hat{\gamma}_a$  possesses a square-root singularity at the leading edge and a square-root zero at the trailing edge. This series necessarily satisfies the steady Kutta condition at the trailing edge. However, as we will now show, this choice of basis expansion leads to invalid results at the endpoints when the aerofoil is permeable.

By sending  $x \rightarrow -1$ , we obtain the asymptotic limits

$$\psi(x)\hat{\gamma}_a(x) \sim \psi(-1)\hat{\gamma}_0 \sqrt{\frac{2}{1+x}}, \quad (3.3.a)$$

$$-\frac{1}{\pi} \int_{-1}^1 \frac{\hat{\gamma}_a(\xi)}{\xi - x} d\xi \sim \Phi^*(x), \quad (3.3.b)$$

$$2 \frac{d\hat{y}_a}{dx}(x) \sim 2 \frac{d\hat{y}_a}{dx}(-1), \quad (3.3.c)$$

where  $\Phi^*(x) = o((1+x)^{-1/2})$  according to (Muskhelishvili 1946, (29.8)). Substitution of these limits into (3.1) results in a contradictory equation where the left-hand side scales like  $(1+x)^{-1/2}$  whereas the right-hand side tends to a constant as  $x \rightarrow -1$ . Asymptotic analysis at the trailing edge generates similar contradictions. Consequently, the Chebyshev expansion generates spurious results at both endpoints, and the  $\hat{\gamma}_n$  coefficients for  $n > 1$  must account for the contradiction, resulting in a slowly converging series. The modification of the square-root behaviour at the endpoints due to porosity

is embedded in the partially-porous aerofoil solution by Iosilevskii (2011, 2013) and is detailed in the generalized porous aerofoil solution by Hajian & Jaworski (2017).

Suppose instead that we do not explicitly enforce the square-root behaviour of  $\hat{\gamma}_a$  at the endpoints, and instead express  $\hat{\gamma}_a$  in the form

$$\hat{\gamma}_a(x) = w^{\alpha, -\beta}(x) \hat{\gamma}_a^*(x), \quad (3.4)$$

where  $w^{a,b}$  represents the weight function

$$w^{a,b}(x) \equiv (1-x)^a (1+x)^b, \quad (3.5)$$

and where  $\hat{\gamma}_a^*(x)$  is a function that is Hölder continuous on  $x \in [-1, 1]$  and is finite and non-zero at  $x = \pm 1$ . The real constants  $\alpha$  and  $\beta$  in (3.4) are unknown and must be found as part of the solution. Using the new expansion (3.4), the limits (3.3.a) and (3.3.b) instead become

$$\psi(x) \hat{\gamma}_a(x) \sim \psi(-1) \hat{\gamma}_a^*(-1) \frac{2^\alpha}{(1+x)^\beta}, \quad (3.6.a)$$

$$-\frac{1}{\pi} \int_{-1}^1 \frac{\hat{\gamma}_a(\xi)}{\xi - x} d\xi \sim -\hat{\gamma}_a^*(-1) \frac{2^\alpha \cot(\pi\beta)}{(1+x)^\beta} + \Phi^*(x), \quad (3.6.b)$$

where now  $\Phi^* = o((1+x)^{-\beta})$ . Accordingly, by matching the singularities in the above two terms through (3.1), we obtain the following expression for  $\beta$ :

$$\beta = \frac{1}{\pi} \cot^{-1}(\psi(-1)) + n, \quad (3.7)$$

for  $n \in \mathbb{Z}$ . A similar procedure at the endpoint  $x = 1$  yields a similar expression for  $\alpha$ :

$$\alpha = \frac{1}{\pi} \cot^{-1}(\psi(1)) + n. \quad (3.8)$$

Consequently, we seek an expansion of the vorticity distribution as a sequence of weighted Jacobi polynomials of the form

$$\hat{\gamma}_a(x) = \hat{\gamma}_0 w^{\alpha, -\beta}(x) + w^{\alpha, 1-\beta}(x) \sum_{n=1}^{\infty} \hat{\gamma}_n P_{n-1}^{\alpha, 1-\beta}(x), \quad (3.9)$$

where  $P_n^{a,b}$  represents the  $n^{\text{th}}$  Jacobi polynomial with parameters  $a$  and  $b$ . The Jacobi polynomials are a classical family of orthogonal polynomials (Szegő 1939) and represent a generalisation of Chebyshev polynomials. Some important properties of the Jacobi polynomials are catalogued in appendix A. This numerical technique is an example of a *spectral method* (Trefethen 2000), where the unknown function is expanded globally in terms of basis functions whose coefficients are chosen by collocation.

Note that the inverse cotangent function in (3.7) and (3.8) decreases monotonically for positive arguments. Therefore, the effect of porosity is to decrease the strength of the both leading-edge singularity and the trailing-edge zero. In the large porosity limit  $\psi(\pm 1) \rightarrow \infty$ , the singularity and zero vanish, and we have  $\alpha = \beta = 0$ . The pressure jump along the chord also vanishes in this limit, as shown by Hajian & Jaworski (2017).

We may now substitute our Jacobi polynomials expansion (3.9) into the singular integral equation (3.1) and collocate at the Jacobi nodes to determine the coefficients  $\hat{\gamma}_n$  following the procedure of Baddoo *et al.* (2019) to furnish a solution to the full unsteady problem.



## 3.2. Unsteady solution

We now seek to adapt the steady solution (3.2) to the full unsteady problem (2.11). The SF-VIE in the unsteady case is distinct from the singular integral equation of the steady case in a number of ways. Firstly, the forcing term  $f_w$  is not regular but possesses a logarithmic singularity at  $x = 1$ . Secondly, the coefficient of  $f_w$  is unknown *a priori* because it is proportional to the aerofoil circulation. Thirdly, the integral equation (2.11) now contains terms of Volterra type. We will now adapt the solution approach in §3.1 to address these issues simultaneously.

We first address the fact that the forcing term  $f_N$  is not regular as  $x \rightarrow 1$  in (2.11). In particular, we may express the forcing contribution from the wake as

$$f_w(x) = \frac{ike^{ikx}}{\pi} G(0, ik(x-1)),$$

where

$$G(s, z) = \int_z^\infty t^{s-1} e^{-t} dt$$

is the incomplete Gamma function. Accordingly, we obtain the asymptotic behaviour (Abramowitz & Stegun 1964)

$$f_w(x) \sim -\frac{ike^{ik}}{\pi} \left( E - \frac{i\pi}{2} + \log(k(1-x)) \right), \quad \text{as } x \rightarrow 1,$$

where  $E$  is the Euler–Mascheroni constant. For the asymptotic matching procedure at the endpoints, we require the left-hand side of (2.11) to possess a logarithmic singularity of the same strength of  $f_w$  at  $x = 1$ . If  $\hat{\gamma}_a$  itself is to be regular, the only way to generate this logarithmic singularity is through the principal value part of the operator  $\mathcal{L}$  (Muskhelishvili 1946). In particular, we require

$$\hat{\gamma}_a \rightarrow -ike^{-ik} \hat{\Omega}, \quad \text{as } x \rightarrow 1.$$

This behaviour may alternatively be derived by enforcing the Kutta condition and requiring the pressure to vanish at the trailing edge in (2.6.a). Accordingly, we adapt the expansion in (3.4) and seek a solution of the form

$$\hat{\gamma}_a(x) = w^{\alpha, -\beta}(x) \hat{\gamma}_a^*(x) + ike^{-ik} 2^{\beta-1} \hat{\Omega} w^{0, 1-\beta}(x), \quad (3.10)$$

where  $f$  is a smooth function. We now note the leading-order asymptotic behaviours as  $x \rightarrow -1$ :

$$\begin{aligned} \int_{-1}^x \hat{\gamma}_a(\xi) d\xi &\sim \frac{(1+x)^{1-\beta}}{1-\beta} \left( 2^\alpha \hat{\gamma}_a^*(-1) + ik 2^{\beta-1} e^{-ik} \hat{\Omega} \right), \\ \psi(x) \hat{\gamma}_a(x) &\sim \frac{\psi(-1)}{(1+x)^\beta} \left( 2^\alpha \hat{\gamma}_a^*(-1) + ik 2^{\beta-1} e^{-ik} \hat{\Omega} \right), \\ -\frac{1}{\pi} \int_{-1}^1 \frac{\hat{\gamma}_a(\xi)}{\xi-x} d\xi &\sim -\frac{\cot(\beta\pi)}{(1+x)^\beta} \left( 2^\alpha \hat{\gamma}_a^*(-1) + ik 2^{\beta-1} e^{-ik} \hat{\Omega} \right), \\ f_a(x) + \hat{\Omega} f_w(x) &\sim f_a(-1) + \hat{\Omega} f_w(-1). \end{aligned}$$

Consequently, we see that the Volterra part of the SF-VIE does not contribute to the asymptotic behaviour at the leading edge, and the expression for  $\beta$  is given by (3.7).

We now inspect the behaviour as  $x \rightarrow 1$  and track terms at higher orders to ensure the correct asymptotic matching. In this limit, we obtain the behaviours

$$\begin{aligned}\hat{\gamma}_a(x) &\sim \hat{\Omega} + \frac{(1-x)^\alpha}{2^\beta} \hat{\gamma}_a^*(1), \\ \int_{-1}^x \hat{\gamma}_a(\xi) d\xi &\sim \int_{-1}^1 \hat{\gamma}_a(\xi) d\xi, \\ -\frac{1}{\pi} \int_{-1}^1 \frac{\hat{\gamma}_a(\xi)}{\xi-x} d\xi &\sim -\frac{ike^{ik}\hat{\Omega}}{\pi} \log(1-x) - \frac{\cot(\alpha\pi)}{2^\beta} (1-x)^\alpha \hat{\gamma}_a(1), \\ f_a(x) + \hat{\Omega} f_w(x) &\sim f_a(1) - \frac{ike^{ik}\hat{\Omega}}{\pi} \left( E - \frac{i\pi}{2} + \log(k(1-x)) \right).\end{aligned}$$

We note that the logarithmic singularities on the third and fourth lines cancel by virtue of the Kutta condition. Furthermore, the constant will be matched through the collocation procedure, so we must choose  $\alpha$  so that the leading-order zero (proportional to  $(1-x)^\alpha$ ) vanishes. Consequently, we obtain the same expression for  $\alpha$  as in (3.8). This result motivates an expansion of  $\hat{\gamma}_a$  of the form

$$\hat{\gamma}_a(x) = w^{0,1-\beta}(x) 2^{\beta-1} A + w^{\alpha,-\beta}(x) \gamma_0 + w^{\alpha,1-\beta}(x) \sum_{n=1}^{\infty} \gamma_n P_{n-1}^{\alpha,1-\beta}(x), \quad (3.11)$$

where

$$A = -ike^{-ik}\hat{\Omega} = -ik\hat{\Gamma}. \quad (3.12)$$

Recall that we do not know the circulation  $\hat{\Gamma}$  *a priori*, which must be determined as part of the solution. However, by using the expansion (3.11), we may express  $\hat{\Gamma}$  in terms of the (also unknown) coefficients to write

$$\hat{\Gamma} = 2AB(2-\beta, 1) + \gamma_0 2^{1+\alpha-\beta} B(1-\beta, 1+\alpha) + \gamma_1 2^{2+\alpha-\beta} B(2-\beta, 1+\alpha), \quad (3.13)$$

where we have used (A 3) to express the integral in terms of the Beta function,  $B$ . Combining (3.12) and (3.13) then yields an equation for  $\hat{\Gamma}$  in terms of the first two coefficients of the Jacobi expansion

$$\hat{\Gamma} = \frac{\gamma_0 2^{1+\alpha-\beta} B(1-\beta, 1+\alpha) + \gamma_1 2^{2+\alpha-\beta} B(2-\beta, 1+\alpha)}{1 + 2ikB(2-\beta, 1)}.$$

It proves convenient to express

$$\hat{\Omega} = \gamma_0 \hat{\Omega}_0 + \gamma_1 \hat{\Omega}_1,$$

so that the SF-VIE equation (2.11) may be expressed in the new form

$$\mathcal{H}[\hat{\gamma}_a](x) = f_N(x), \quad (3.14)$$

where the new, regularised operator  $\mathcal{H}$  is defined as

$$\mathcal{H}[\hat{\gamma}_a](x) := \mathcal{L}[\hat{\gamma}_a](x) - \left( \hat{\gamma}_0 \hat{\Omega}_0 + \hat{\gamma}_1 \hat{\Omega}_1 \right) f_C(x).$$

It is straightforward to verify that the regularised operator  $\mathcal{H}$  takes a bounded value at the endpoints. Following the procedure detailed in Baddoo *et al.* (2019), we may now truncate the infinite sum in (3.11) at  $N$  and collocate equation (3.14) at the zeros of the

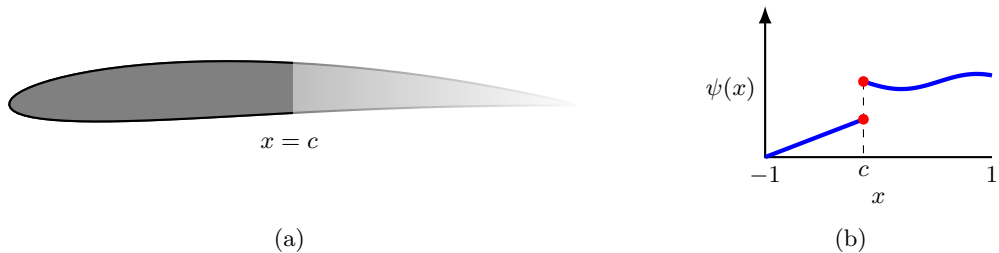


Figure 2: Example of an aerofoil with a discontinuous porosity distribution, where the discontinuity occurs at dimensionless chordwise position  $x = c$ . (a) Illustration of an aerofoil with an discontinuous porosity distribution, where the porosity variation along the chord is indicated by a colour gradient. (b) A representative discontinuous porosity distribution. Note that the porosity along the forward section need not be constant.

Jacobi polynomial  $P_{N+1}^{\alpha, -\beta}$  to construct an  $(N + 1) \times (N + 1)$  system of linear equations for the coefficients  $\hat{\gamma}_n$ .

In carrying out the collocation procedure, it is useful to note that the effect of the operator  $\mathcal{L}$  on each individual weighted Jacobi polynomial can be computed using standard functions. For example,

$$\mathcal{L} [w^{a,b}(x)P_n^{a,b}(x)](x) = ik\psi(x)I_n^{a,b}(x) + \psi(x)w^{a,b}(x)P_n^{a,b}(x) - \frac{w^{a,b}(x)}{\pi}Q_n^{a,b}(x)$$

where  $I_n^{a,b}$  is the integral of the weighted Jacobi (see (A 6)) and  $Q_n^{a,b}$  is the associated Jacobi function of the second kind (see (A 4)).

Finally, we point out that an alternative weight function should be used for higher-accuracy solutions. For uniformly porous aerofoils with constant  $\psi$ , the Jacobi weight function precisely captures the behaviour at the endpoints. However, for non-constant porosity profiles, the weight function should be written more generally as

$$(1 - x)^{\alpha(x)}(1 + x)^{\beta(x)}, \quad (3.15)$$

where  $\alpha$  and  $\beta$  are regular  $x = \pm 1$  (Hajian *et al.* 2018). Although a set of orthogonal polynomials could in principle be constructed with weight function (3.15) via Gram–Schmidt orthogonalisation, we find it more appropriate to use the weight function (3.5) with the Jacobi polynomials due to the existence of many useful identities (see appendix A) and practical ease of computation. Whilst this choice precludes the possibility of spectral accuracy, only a few polynomials are usually required to obtain a degree of accuracy that is finer than the size of other physical quantities that are being ignored.

We now present several extensions to the method that enable the calculation of the vorticity distribution, including the case where the porosity distribution is discontinuous. The numerical method verifies the solution for quasi-steady aerodynamics and establishes both the circulatory and non-circulatory vorticity distributions for generalized unsteady aerodynamics of porous aerofoils.

### 3.3. Solution for discontinuous porosity distributions

The case of a discontinuous porosity profile is now considered. This scenario is motivated in part by the investigation by Geyer & Sarradj (2014), who showed that, depending on the porous material, aerofoils with porosity at the trailing-edge section only can still lead to a noticeable noise reduction, while maintaining a certain level of aerodynamic performance over a fully-porous aerofoil. A schematic of a partially-porous aerofoil is

illustrated in figure 2. When the discontinuity is located at  $x = c$ , the original SF-VIE (2.11) may be partitioned into two parts:

$$\psi_l(x) \left[ \hat{\gamma}_a(x) + ik \int_{-1}^x \hat{\gamma}_a(\xi) d\xi \right] - \frac{1}{\pi} \int_{-1}^1 \frac{\hat{\gamma}_a(\xi)}{\xi - x} d\xi = f_a(x) + \hat{\Omega} f_w(x), \quad -1 < x < c, \quad (3.16.a)$$

$$\psi_r(x) \left[ \hat{\gamma}_a(x) + ik \int_{-1}^x \hat{\gamma}_a(\xi) d\xi \right] - \frac{1}{\pi} \int_{-1}^1 \frac{\hat{\gamma}_a(\xi)}{\xi - x} d\xi = f_a(x) + \hat{\Omega} f_w(x), \quad c < x < 1, \quad (3.16.b)$$

where the subscripts l and r correspond the left and right sides of the discontinuity so that  $\psi_l(c^-) \neq \psi_r(c^+)$ . We only consider the case where the porosity increases across the discontinuity so that  $\psi_l(c^-) < \psi_r(c^+)$ . If the porosity decreases across discontinuity, then the pressure gradient possesses a singularity at the junction  $x = c$ . These singularities are unphysical (except when the singularity is at the leading edge) and therefore we do not consider this case further.

We require the pressure jump across the wing to vanish at  $x = c$  to ensure that there is no discontinuity in the seepage velocity (2.3). In particular, asymptotic analysis close to the discontinuity (Baddoo *et al.* 2019) reveals that

$$\left| \hat{\gamma}_a(x) + ik \int_{-1}^x \hat{\gamma}_a(\xi) d\xi \right| \sim |x - c|^\lambda \hat{\gamma}_a^*(x), \quad \text{as } x \rightarrow c,$$

where

$$\lambda = \frac{1}{\pi} [\cot^{-1}(\psi_l(c^-)) - \cot^{-1}(\psi_r(c^+))],$$

and where  $\hat{\gamma}_a^*(x)$  is regular in  $-1 < x < c$  and  $c < x < 1$  but may be discontinuous at  $x = c$ . Since we assumed that the porosity is increasing across the discontinuity, we have  $\lambda > 0$  and the pressure therefore vanishes at the junction. This motivates two separate expansions for  $\hat{\gamma}_a$  in the left and right regions of the form

$$\hat{\gamma}_l(\tau_l) = \hat{\gamma}_{l,0} w^{\lambda, -\beta}(\tau_l) + 2^{\beta-1} \Pi w^{0, 1-\beta}(\tau_l) + w^{\lambda, 1-\beta}(\tau_l) \sum_{n=1}^{\infty} \hat{\gamma}_{l,n} P_{n-1}^{\lambda, 1-\beta}(\tau_l), \quad (3.17.a)$$

$$\hat{\gamma}_r(\tau_r) = 2^{-\alpha} \Lambda w^{\alpha, 0}(\tau_r) + \Lambda w^{0, \lambda}(\tau_r) + w^{\alpha, \lambda}(\tau_r) \sum_{n=1}^{\infty} \hat{\gamma}_{r,n} P_{n-1}^{\alpha, \lambda}(\tau_r), \quad (3.17.b)$$

where  $\Pi$  and  $\Lambda$  are constants and we have introduced the rescaled variables

$$\begin{aligned} \tau_l(x) &= -1 + 2 \frac{x+1}{1+c}, & -1 < x < c, \\ \tau_r(x) &= 1 + 2 \frac{x-1}{1-c}, & c < x < 1, \end{aligned}$$

so that  $-1 < \tau_l, \tau_r < 1$ . We now seek to express the constants  $\Pi$  and  $\Lambda$  in terms of the unknown coefficients  $\hat{\gamma}_{l,n}$  and  $\hat{\gamma}_{r,n}$ . Beginning with the constant  $\Pi$ , we note the two relations

$$\hat{\gamma}_a(c) = \Pi, \quad \text{and} \quad \hat{\gamma}_a(c) = -ik \int_{-1}^c \hat{\gamma}_a(\xi) d\xi.$$

The latter expression may be evaluated using the expansion (3.17.a) and the quadrature formula (A 3). A simple rearrangement then allows us to express  $\Pi$  in terms of  $\hat{\gamma}_{l,0}$  and

$\hat{\gamma}_{1,1}$  as

$$\Pi = \Pi_0 \hat{\gamma}_{1,0} + \Pi_1 \hat{\gamma}_{1,1},$$

where

$$\Pi_0 = \frac{-ik(1+c)2^{1-\beta+\lambda}B(2-\beta, 1+\lambda)}{1+ik(1+c)B(2-\beta, 1)}, \quad \Pi_1 = \frac{-ik(1+c)2^{-1/2+\lambda}B(1/2, 1+\lambda)}{1+ik(1+c)B(2-\beta, 1)}.$$

We now seek to express  $\Lambda$  in terms of the coefficients  $\hat{\gamma}_{1,n}$  and  $\hat{\gamma}_{r,n}$ . By employing a similar approach to §3.2, it is straightforward to show that the new expression for  $\Lambda$  is

$$\Lambda = A_{1,0} \hat{\gamma}_{1,0} + A_{1,1} \hat{\gamma}_{1,1} + A_{r,1} \hat{\gamma}_{r,1},$$

where

$$\begin{aligned} A_{1,0} &= \mathcal{M} \times \left[ (1+c) (\Pi_0 B(2-\beta, 1) + 2^{-\beta+\lambda} B(1-\beta, 1+\lambda)) + (1-c) \Pi_0 B(1, 1+\alpha) \right], \\ A_{1,1} &= \mathcal{M} \times \left[ (1+c) (\Pi_1 B(2-\beta, 1) + 2^{1-\beta+\lambda} B(2-\beta, 1+\lambda)) + (1-c) \Pi_1 B(1, 1+\alpha) \right], \\ A_{r,1} &= \mathcal{M} \times (1-c) 2^{\alpha+\lambda} B(1+\alpha, 1+\lambda), \\ \mathcal{M} &= \frac{-ik2^{-\lambda}}{1+ik(1-c)B(1, 1+\lambda)}. \end{aligned}$$

We may now substitute the expansions (3.17.b) and (3.17.a) into (3.16.a) and (3.16.b). By collocating the Jacobi nodes on the forward and aft sections, we may obtain a system of linear equations for the unknown coefficients. During the procedure we encounter the Cauchy integral of the weighted Jacobi polynomials, which can be calculated using (A 5).

Although only a single discontinuity was considered in this example, any finite number of discontinuities could be modelled using the same approach.

### 3.4. Circulatory and non-circulatory solutions

The solution to the full unsteady problem in §3.2 may be separated into circulatory and non-circulatory parts by writing

$$\hat{\gamma}_a(x) = \hat{\gamma}_a^C(x) + \hat{\gamma}_a^N(x), \quad (3.18)$$

where the superscripts  $C$  and  $N$  denote the circulatory and non-circulatory contributions, respectively. The circulatory part is sometimes referred to the wake-induced component because it contains information about the effect of the downstream wake on the aerofoil motion. Conversely, the non-circulatory part is sometimes referred to as the added mass component, as it represents the effects of the unsteady sloshing of the flow about the aerofoil. Recent research into the origin of added mass led Leonard & Roshko (2001) and Eldredge (2010) to postulate that its associated force may be represented solely by inviscid theory, even in viscous and separated flows. Corkery *et al.* (2019) confirmed experimentally the ability of inviscid theory to represent added mass effects as a non-circulatory component that depends only on body geometry and its motion, where the circulatory terms in turn measure the viscous effects associated with the bound vorticity and the wake. The circulatory and non-circulatory components combine to give the full vorticity distribution on the aerofoil.

As its name suggests, the non-circulatory component is the solution to (2.11) subject

to the auxiliary requirement that its net sum over the aerofoil is identically zero,

$$\int_{-1}^1 \hat{\gamma}_a^N(\xi) d\xi = 0. \quad (3.19)$$

The problem of finding  $\hat{\gamma}_a^N$  subject to the SF-VIE (2.11) and to both the non-circulatory condition (3.19) and the Kutta condition is generally ill-posed. Consequently, we must relax the Kutta condition in the circulatory and non-circulatory parts and permit singularities at the trailing-edge in both  $\hat{\gamma}_a^C$  and  $\hat{\gamma}_a^N$ . These singularities are perfectly valid (for example, they appear in the impermeable case detailed in (Bisplinghoff *et al.* 1996, §5-6)) provided that they cancel when combined in (3.18).

It is simpler to derive the non-circulatory solution and then use the full solution and (3.18) to determine the circulatory solution. Following the analysis of §3.2, we seek an expansion of the form

$$\hat{\gamma}_a^N(x) = \Theta w^{\alpha-1, 1-\beta}(x) + w^{\alpha, -\beta}(x) \gamma_0^N + w^{\alpha, 1-\beta}(x) \sum_{n=1}^{\infty} \gamma_n^N P_{n-1}^{\alpha, 1-\beta}(x),$$

where

$$\Theta = \frac{-\gamma_0^N 2^{1+\alpha-\beta} B(1+\alpha, 1-\beta) - \gamma_1^N 2^{2+\alpha-\beta} B(1+\alpha, 2-\beta)}{2^{1+\alpha-\beta} B(\alpha, 2-\beta)}.$$

Now a similar collocation scheme to §3.2 can be employed to determine the coefficients  $\gamma_n^N$ .

### 3.5. Quasi-steady solution

The quasi-steady problem is equivalent to the steady problem described in Hajian & Jaworski (2017) with the exception that the kinematic boundary condition is replaced by the instantaneous unsteady boundary condition (2.8). Accordingly, the singular integral equation (2.9) becomes

$$\psi(x) \hat{\gamma}_a^Q(x) - \frac{1}{\pi} \int_{-1}^1 \frac{\hat{\gamma}_a^Q(\xi)}{\xi - x} d\xi = -2 \left( ik \hat{y}_a(x) + \frac{d\hat{y}_a}{dx}(x) \right), \quad (3.20)$$

where the superscript  $Q$  denotes the quasi-static solution. This singular integral equation may be solved analytically using classical techniques (Muskhelishvili 1946). The solution space may be closed by enforcing the Kutta condition and the corresponding solution is

$$\hat{\gamma}_a^Q(x) = \frac{-2}{1 + (\psi(x))^2} \left\{ \psi(x) \left( ik \hat{y}_a(x) + \frac{d\hat{y}_a}{dx}(x) \right) + \frac{Z(x)}{\pi} \int_{-1}^1 \left( ik \hat{y}_a(\xi) + \frac{d\hat{y}_a}{dx}(\xi) \right) \frac{d\xi}{Z(\xi)(\xi - x)} \right\}, \quad (3.21)$$

where  $k(x) = (1/\pi) \cot^{-1}(\psi(x))$  and

$$Z(x) = \sqrt{1 + (\psi(x))^2} \exp \left[ \int_{-1}^1 \frac{k(\xi)}{\xi - x} d\xi \right].$$

In special cases, such as uniformly porous aerofoils with simple geometries, the singular integrals in (3.21) can be calculated analytically, and the full solution can be expressed in closed form. Otherwise, the solution in (3.21) contains nested singular integral equations that must be computed numerically using Gauss–Jacobi quadrature.

## 4. Results

In this section we present a collection of aerodynamic results to showcase the versatility of our numerical scheme and to extend the classical unsteady aerodynamic analyses of Theodorsen and Sears to include the effects of porosity. These results also offer physical insight into the underlying flight mechanisms utilised by porous wings. Although the numerical scheme is valid for aerofoils of arbitrary (thin) shape, we focus on symmetric aerofoils undergoing pitching and heaving motions. Consequently, we follow Moore (2014) and write the mean camber line as

$$y_a(x, t) = \left( \frac{1}{2}\beta_0 + \beta_1 x \right) e^{ikt}.$$

The amplitude of the leading-edge is therefore given by the (real) number

$$A = \frac{1}{2}\beta_0 - \beta_1,$$

so that  $\beta_1 = \beta_0/2$  represents pure pitching motions, whereas  $\beta_1 = 0$  represents pure heaving motions.

Physical considerations demand additionally that the analysis in this section is restricted to the case where the leading edge is impermeable, i.e.  $\psi(-1) = 0$ . The seepage velocity is proportional to the pressure gradient by Darcy's law (2.3) and the proportionality function is the porosity distribution. Since the pressure gradient possesses a singularity at the leading edge, the seepage velocity therefore also possesses a singularity at the leading-edge *unless* the proportionality function vanishes at  $x = -1$ . If  $\psi(-1) \neq 0$ , then the seepage velocity near the trailing-edge will be large. However, a large seepage velocity is in violation of the modelling assumptions for Darcy's law, which effectively models the pore-scale flow as a Stokes flow. Accordingly, in order to obtain physically faithful results, we focus on the case  $\psi(-1) = 0$ , although the mathematical analysis remains valid in other cases.

### 4.1. Pressure distributions

We now consider a set of examples to illustrate the effects of porosity on the pressure difference across the chord. We first consider aerofoils with continuous porosity distributions and then consider aerofoils with discontinuous porosity distributions.

#### 4.1.1. Continuous porosity distributions

The numerical method in §3 is amenable to any continuous porosity distribution. Figure 3 compares pressure distributions for aerofoils with linear and parabolic porosity distributions undergoing pitching or heaving motions. The Kutta condition is clearly satisfied at the trailing edge for all cases presented. Figure 3 indicates that the introduction of porosity decreases the pressure jump across the aerofoil under both pitching and heaving motions. As the porosity increases along the chord, the pressure distribution decreases except in a small region localised to the trailing edge. This reduction corresponds to a significant reduction in the unsteady lift. For example, the pressure distribution along an impermeable heaving aerofoil shown in figure 3b possesses an interior stationary point at  $x = 0$ , which is characteristic of these dynamics (Wu 1961). The effect of increasing the magnitude of the aerofoil porosity is to shift this turning point nearer the leading edge, whilst simultaneously reducing the magnitude of the pressure jump there. We also note the rapid changes in pressure at the trailing edge  $x = 1$ , which is caused by the reduction in the strength of the trailing-edge zero by (3.8). This behaviour is associated with the reduction in vortex shedding at the porous trailing edge.

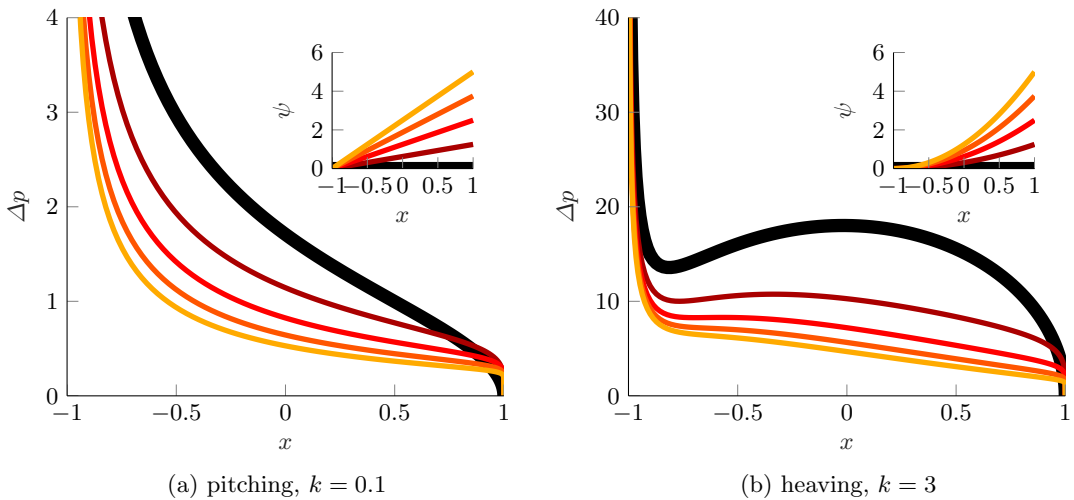


Figure 3: Pressure distributions for a porous aerofoil undergoing unsteady motions with continuous porosity distributions: (a) pitching about  $x = -1$  at  $k = 0.1$  with linear porosity gradient; (b) heaving at  $k = 3$  with parabolic porosity gradient. The impermeable limit is indicated by the thick black line.

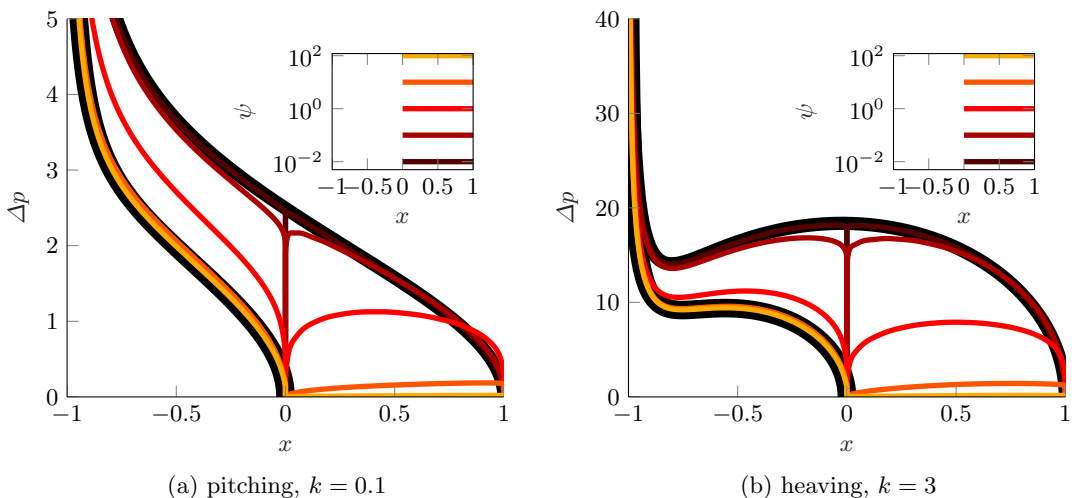


Figure 4: Pressure distributions on a partially-porous aerofoil undergoing pitching or heaving motions. The impermeable cases for a full aerofoil and a truncated aerofoil are illustrated by the thick black lines. The porosity distributions are plotted on a logarithmic scale in the figure insets, where  $\psi = 0$  for  $x < 0$ .

#### 4.1.2. Discontinuous porosity distributions

The numerical method in §3 is now applied to aerofoils with discontinuous porosity distributions. Specifically, the numerical scheme is demonstrated for aerofoils with an impermeable leading edge section for  $x < 0$  and a constant-porosity section for  $x > 0$ . Figure 3 plots the surface pressure jump for pitching motions at  $k = 0.1$  about  $x = -1$  and heaving motions at  $k = 3$ . The seepage velocity is continuous across the chord, as



evidenced by the vanishing jump at pressure located at the junction  $x = 0$ . Note that even a small amount of porosity is sufficient to enforce a zero pressure jump at the junction.

For both the pitching and plunging cases and at different reduced frequencies, when the porosity is large the pressure jump along the permeable section vanishes. Accordingly, the permeable section of the wing behaves effectively as an extension of the wake: although the pressure jump vanishes, the vorticity distribution does not, by (2.6.a). For these cases with an impermeable forward section, the aerofoil solution for large porosity in the aft section is the same as the solution of an impermeable aerofoil truncated at  $x = c$ , i.e. the solution attained as rescaling the characteristic length scale by a factor of  $(c + 1)/2$ , or equivalently, using the mappings

$$x \mapsto \frac{(c + 1)x + (c - 1)}{2}, \quad y_a(x) \mapsto \frac{c + 1}{2}y_a, \quad k \mapsto k\frac{c + 1}{2}.$$

#### 4.2. Theodorsen function

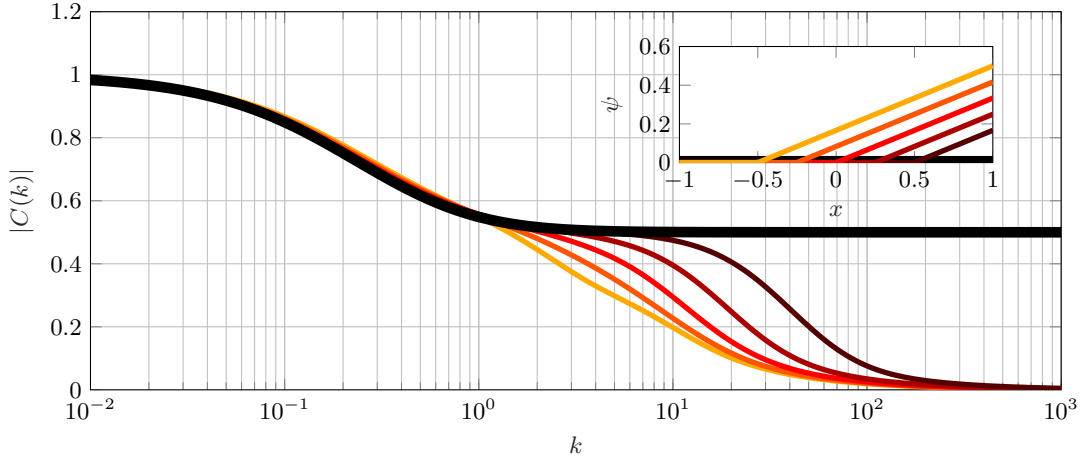
The Theodorsen function (Theodorsen 1935) may be interpreted the ratio of the wake-induced (circulatory) lift  $L^C$  to the quasi-steady lift  $L^Q$  (cf. Bisplinghoff *et al.* 1996, pp. 279),

$$C(k) = \frac{L^C}{L^Q} = \frac{K_1(ik)}{K_0(ik) + K_1(ik)},$$

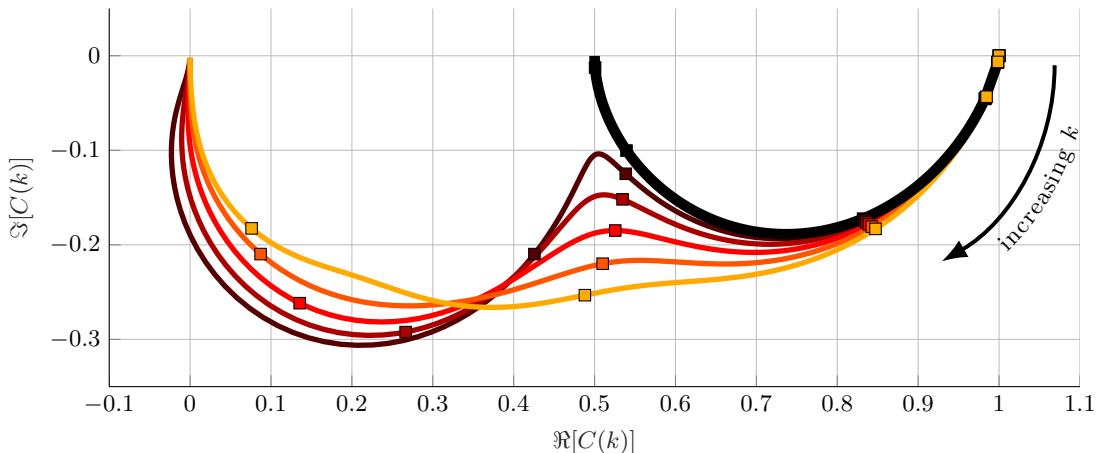
where  $K_0$  and  $K_1$  are modified Bessel functions of the second kind. The lack of an analytic solution to SF-VIE (2.11) precludes the derivation of a similar expression for the permeable case in terms of standard functions. However, we may use the numerical solution presented in §3 to compute the relevant circulatory and quasi-steady lift quantities to construct numerically a porous extension to the Theodorsen function. Specifically, the wake-induced lift is computed by the numerical scheme in §3.4, whereas the quasi-steady lift may be determined analytically using the solution presented in §3.5.

Figure 5 illustrates the computed Theodorsen function for a heaving flat plate with a range of piecewise-linear porosity profiles. We see that the magnitude of the Theodorsen function for porous aerofoils is almost uniformly bounded above by the original, impermeable Theodorsen function, as illustrated in figure 5a. Given that porosity cannot increase the magnitude of the quasi-steady lift, figure 5a implies that an effect of porosity is to substantially reduce the wake-induced lift, which is in accordance with the hypothesis that an effect of trailing-edge porosity is to reduce the amount of vorticity shed into the wake. The mathematical feature by which this occurs is through the reduction of the trailing-edge zero in the pressure distribution via (3.8).

As the reduced frequency increases, the numerically-computed Theodorsen curves depart dramatically from the traditional impermeable solution. In particular, the ratio between the wake-induced lift and quasi-steady lift vanishes with increasing frequency. There is a delicate balance between these two lift quantities in the impermeable case so that their ratio tends to 1/2 in the large frequency limit. This balance is broken when porosity is introduced. In particular, the porous trailing edges used in figure 5 effectively reduce the amount of vorticity shed into the wake by reducing the pressure jump at the trailing edge. Therefore, the effect of porosity is to decrease the wake-induced lift. Moreover, the curves in figure 5 show that the wake-induced lift is reduced at a greater rate than the reduction in the quasi-steady lift. However, we note that the large frequency limit is beyond the validity of the mathematical modelling employed in this paper: as discussed by Howe (1979) and noted more recently by Weidenfeld & Manela (2016), the present modelling assumptions for porosity are only valid when there is Stokes flow in the



(a) Absolute value of the Theodorsen function as a function of frequency. The inset axis shows the porosity distributions.



(b) Porous extension of the Theodorsen function in the spectral plane.

Figure 5: Theodorsen function for aerofoils with linear porosity gradients. The colours correspond to the porosity profiles illustrated in the inset axes in (a). In particular, the black curve represents an impermeable aerofoil. The points  $k = 0, 10^{-3}, 10^{-2}, 10^{-1}, 1, 10$  are indicated by  $\square$  with  $k = 0$  representing the rightmost part of the curve.

pores passing through the wing, which is rendered invalid at large frequencies. We expect that a higher-order (e.g., quadratic) porosity law would yield more physically meaningful results at high frequencies; an exploration of such porosity models is beyond the scope of the present work and is not pursued here.

#### 4.3. Gust response

We now consider a uniform flow in the horizontal direction with a transverse sinusoidal gust in the vertical direction, as illustrated in figure 6. The gust is convected at the free-stream velocity and has unit amplitude. The interaction between the gust and the aerofoil

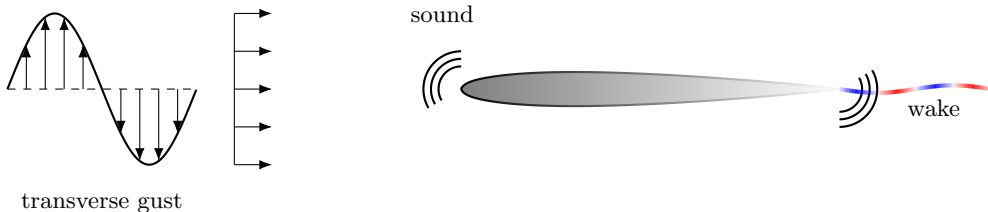


Figure 6: The harmonic gust response problem considered by Sears (1941). A symmetric, stationary, porous aerofoil is subjected to an unsteady vertical sinusoidal disturbance convected at the velocity of the freestream, resulting in unsteady wake generation. Acoustic waves are also generated that can be modelled using the Sears response function.

generates unsteady lift, as well as pressure perturbations that propagate to the acoustic far field as sound waves.

The Sears function (Sears 1941) is the unsteady lift response function to a harmonic gust and may be written in the form

$$S(k) = C(k) [J_0(k) - iJ_1(k)] + iJ_1(k), \quad (4.1)$$

for a gust of frequency  $k$ , where  $J_n$  are Bessel functions of the first kind of order  $n$ . Like the relationship between the Theodorsen and Wagner functions, the Sears harmonic gust response function is connected via the Fourier transform to the Küssner sharp-edged gust function, which can be used to predict the aerodynamic response to arbitrary linear gusts by appeal to Duhamel's integral.

For a gust of unitary amplitude, the porous boundary condition (2.2) is

$$w(x, t) = w_s(x, t) - e^{ik(t-x)}.$$

Therefore, the forcing function  $f_a$  in the SF-VIE becomes

$$f_a(x) = e^{-ikx},$$

and we may apply the numerical scheme developed in §3. Whilst the Volterra part of the SF-VIE renders it impossible to find analytic forms for the Sears function, our numerical scheme is sufficiently fast and robust that we may produce an accurate approximation for a range of porosity gradients.

We now explore the effects of aerofoil porosity on the gust response function in figure 7. Both continuous and discontinuous profiles are considered and are illustrated in the inset plot of figure 7a. The porosity distribution has a fixed value of unity at the trailing edge for all cases considered, and the permeable length of the aerofoil is varied. We first plot the unsteady lift normalised by the quasi-steady lift on an impermeable aerofoil (i.e.,  $-4\pi$ ) in figure 7a. The results show that the magnitude of the unsteady lift is almost always less than that of the impermeable aerofoil. Porosity allows seepage flow through the aerofoil surface, thereby reducing the pressure jump across the wing. This effect translates to a reduction in the unsteady lift, which would also correlate, for example, to reductions in far-field sound.

Contrary to expectations, there is little difference between the unsteady lift for the continuous and discontinuous porosity profiles: the solid and dashed lines indicating

these results are virtually coincident in figures 7a and 7b. Whilst other studies (Kisil & Ayton 2018) have determined that the permeable-impermeable junction is an additional source of pressure scattering, the discontinuity does not appear to play a significant role in this case.

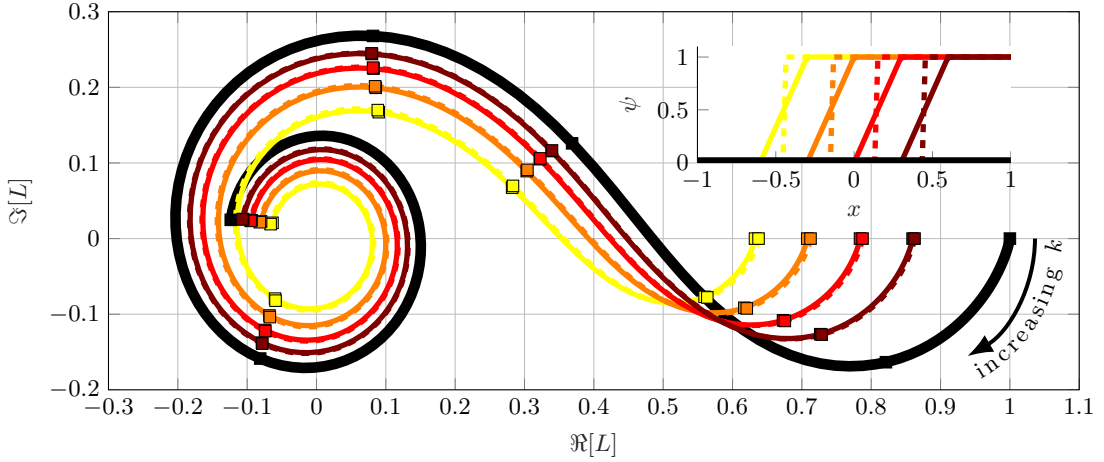
Instead of normalising the unsteady lift by the unsteady lift of the impermeable aerofoil as in figure 7a, we may instead normalise by the quasi-steady lift for each individual porous aerofoil. This ratio – the Sears function generalised for porous aerofoils – is illustrated in figure 7b. Under this rescaling, we now see that there are far fewer differences between the corresponding lift curves. This suggests that, to a high degree of accuracy, the unsteady lift for any frequency can be calculated for that aerofoil by using the Sears function using the quasi-steady lift for the aerofoil. Analytic expressions for the quasi-steady lift are available in §3.5.

## 5. Conclusions

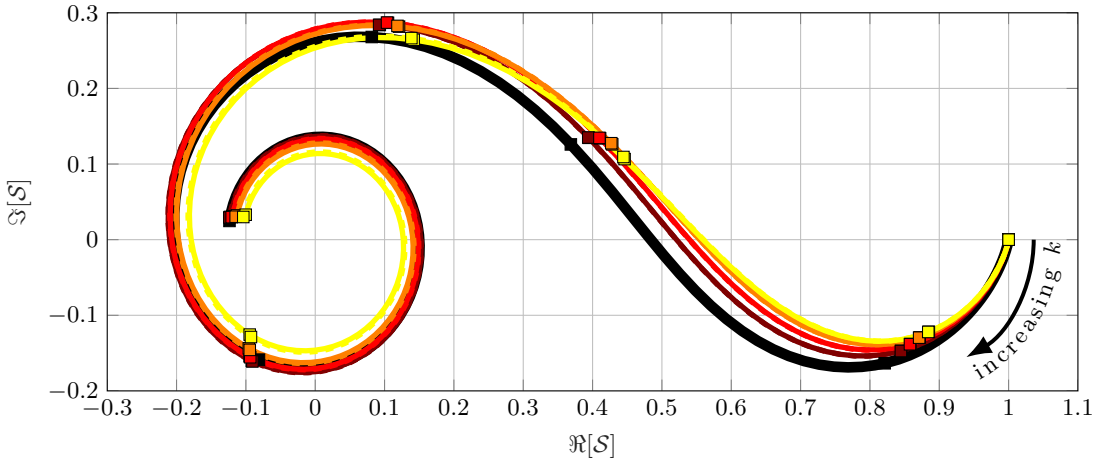
A comprehensive unsteady aerodynamic theory is presented for lifting porous bodies. The aerodynamic problem is modelled as a singular Fredholm–Volterra integral equation, which is solved numerically using a new method developed in this paper. The foundation of this method relies on the Jacobi polynomial solution technique; the bound vorticity distribution is expanded as a series of weighted Jacobi polynomials whose parameters are determined by asymptotic analysis at the endpoints of the aerofoil. The numerical method therefore remains accurate at the endpoints, which is important when imposing the Kutta condition and in the computation of the leading-edge suction. The aerodynamic solution converges rapidly and is straightforward to implement for both continuous and discontinuous porosity distributions.

The new numerical scheme enables the porous extension of the classical works by Theodorsen (1935) for harmonic aerofoil motions and Sears (1941) for harmonic gusts. Specifically, the impermeable surface boundary condition is relaxed to include the effects of Darcy-type chordwise porosity gradients. The porous extension of the Theodorsen function is investigated for a heaving flat plate, where the porous results depart distinctly from the traditional impermeable solution and have a limiting value of zero at large reduced frequency. The magnitudes of the circulatory and quasi-steady lift are both reduced by porosity, although the reduction in circulatory lift is larger with increasing reduced frequency. The reason for this behaviour is that the porous trailing edge effectively reduces the amount of vorticity shed into the wake by decreasing the pressure jump at the trailing edge; porosity decreases the wake-induced lift. Porosity also plays a significant role in the reduction of unsteady lift in response to a gust, although the jump discontinuity of porosity distribution along the aerofoil does not appear to affect the unsteady lift in comparison to smooth distributions. In contrast to the notable impact of porosity on the Theodorsen function for aerofoil motions, the Sears gust response function is relatively insensitive to the porosity distributions considered here, as well as over a range of reduced frequencies and for pure pitching or heaving motions.

The analysis presented in this paper invites companion experimental studies for validation and to suggest appropriate model refinements as required. The present work restricts its attention to linear, Darcy-type porosity profiles. Whilst this approach is valid when the Reynolds number of the flow through the pores is small, a higher-order quadratic model such as the Ergun (1952) model may prove more appropriate in practice, especially near the leading edge where the pressure gradient is large. The analysis of Wegert *et al.* (1987) for steady flow through a cylindrical shell indicates that nonlinear porosity functions lead to a nonlinear Riemann–Hilbert problem, which can be solved using an iterative technique



(a) Unsteady lift normalized by quasi-steady lift from impermeable aerofoil.



(b) Porous extension of the Sears function in the spectral plane.

Figure 7: Sears function for porous aerofoils: (a) unsteady lift normalized by the quasi-steady value of  $-4\pi$  for impermeable aerofoils; (b) Sears function aerofoils with continuous (—) and discontinuous (---) porosity distributions. The colours corresponds to the porosity profiles illustrated in the inset axes in (a). The points  $k = 0, 0.1, 1, 2, 5, 10$  are indicated by  $\square$ , whilst  $k = 0$  is indicated on the rightmost part the curve.

(Wegert 1990). Future work will be devoted to the adaptation of the current study to more general, nonlinear porosity functions to improve the physical fidelity of the present model, possibly through the formulation of an appropriate nonlinear Riemann–Hilbert problem.

The numerical approach advocated in the present research is sufficiently fast and accurate to be integrated into design optimisation routines. In particular, it is often desirable to reduce aeroacoustic emissions with a minimal aerodynamic penalty (Jaworski & Peake 2013, 2020). Initial assessment of this performance trade-off was explored by

Weidenfeld & Arad (2018) in the case of an elastic aerofoil, and optimization of elastic aerofoil effects on unsteady propulsion by Moore (2015) found that the limiting case of a torsional spring at the leading edge of the wing led to optimal thrust conditions. More broadly, the inclusion of elastic effects is an important step forward in improving the physical fidelity of the mathematical modelling that may also contribute to biologically-inspired problems in unsteady flows. For example, the Jacobi polynomial approach of the present work may be adapted into the analysis of Tzezana & Breuer (2019) to consider porous, compliant wings. Similarly, the study of emergent motions of fliers and swimmers by Moore (2014) may also be extended to include porous planform effects by using the numerical scheme developed here.

## Acknowledgement

P. J. B. was supported by EPSRC grant no. 1625902. J. W. J. gratefully acknowledges the financial support of the National Science Foundation under grant awards 1805692 and 1846852. R. H. acknowledges the generous support of the David Crighton Fellowship from DAMTP, University of Cambridge. P. J. B. and J. W. J. would like to thank the Isaac Newton Institute for Mathematical Sciences, Cambridge, for support during the programme ‘‘Bringing pure and applied analysis together via the Wiener–Hopf technique, its generalisations and applications’’ where some work on this paper was undertaken. This programme was supported by EPSRC grant no EP/R014604/1.

## Declaration of interests

None.

## Appendix A. Identities for Jacobi polynomials

This appendix compiles some useful identities for Jacobi polynomials. All of the relations presented assume that  $a, b > -1$ . The Jacobi polynomials are normalised so that

$$P_0^{a,b}(x) = 1.$$

Higher-order polynomials may be calculated using the recurrence relation

$$\begin{aligned} & 2n(n+a+b)(2n+a+b-2)P_n^{a,b}(x) \\ &= (2n+a+b-1)\left\{(2n+a+b)(2n+a+b-2)x+a^2-b^2\right\}P_{n-1}^{a,b}(x) \\ & \quad -2(n+a-1)(n+b-1)(2n+a+b)P_{n-2}^{a,b}(x), \end{aligned} \quad (\text{A } 1)$$

for  $n = 2, 3, \dots$ , where we have used the convention that  $P_{-1}^{a,b}(x) \equiv 0$ .

The Jacobi polynomials satisfy the general orthogonality relation

$$\int_{-1}^1 P_m^{a,b} P_n^{a,b} w^{a,b}(x) dx = \frac{2^{a+b+1}}{2n+a+b+1} \cdot \frac{G(n+a+1)G(n+b+1)}{n!G(n+a+b+1)} \delta_{mn}, \quad (\text{A } 2)$$

where  $G$  is the Gamma function. In particular, when  $m = n = 0$ , we have

$$\int_{-1}^1 w^{a,b}(x) dx = 2^{1+a+b} B(1+b, 1+a), \quad (\text{A } 3)$$

where  $B(\cdot, \cdot)$  is the Beta function.

Analytic expressions of the finite Hilbert transform of the weighted Jacobi polynomials are (Polyanin 1998, p. 797)

$$\begin{aligned} \int_{-1}^1 w^{a,b}(t) \cdot \frac{P_n^{a,b}(t)}{t-x} dt &= \frac{\pi w^{a,b}(x) P_n^{a,b}(x)}{\tan(\pi a)} \\ &\quad - 2^{a+b} B(n+b+1, a) \cdot {}_2F_1 \left[ \begin{matrix} n+1, -n-a-b \\ 1-a \end{matrix}; \frac{1-x}{2} \right], \\ &:= w^{a,b}(x) Q_n^{a,b}(x). \end{aligned} \quad (\text{A } 4)$$

We also require the transform when the principal value part is not assumed. The identity for the zeroth Jacobi polynomial is (Grosjean 1986, Eqs. 12 & 13)

$$\begin{aligned} \int_{-1}^1 \frac{w^{a,b}(t)}{t-x} dt &= \frac{2^{a+b+1} G(a+1) G(b+1)}{G(a+b+2)} \\ &\quad \times \begin{cases} \frac{1}{x-1} \cdot {}_2F_1 \left[ \begin{matrix} a+1, 1 \\ a+b+2 \end{matrix}; \frac{2}{1-x} \right], & |x-1| > 2, \\ \frac{1}{x+1} \cdot {}_2F_1 \left[ \begin{matrix} b+1, 1 \\ a+b+2 \end{matrix}; \frac{2}{1+x} \right], & |x+1| > 2, \end{cases} \end{aligned} \quad (\text{A } 5)$$

and the corresponding results for the higher-order polynomials can be obtained through the recurrence relation (A 1).

Finally, the partial integral of a weighted Jacobi polynomial is (DLMF 2019, Eq. 18.17.1)

$$\begin{aligned} \int_{-1}^x w^{a,b}(y) P_n^{a,b}(y) dy &= \begin{cases} -\frac{w^{a+1,b+1}(x)}{2n} P_{n-1}^{a+1,b+1}(x), & n > 0, \\ 2^{1+a+b} B \left( \frac{1+x}{2}; 1+b, 1+a \right), & n = 0, \end{cases} \\ &:= I_n^{a,b}(x) \end{aligned} \quad (\text{A } 6)$$

where  $B(\cdot; \cdot, \cdot)$  is the incomplete Beta function.

## REFERENCES

- ABDOU, M. A. 2003 Fredholm-Volterra integral equation with singular kernel. *Appl. Math. Comput.* **137** (2-3), 231–243.
- ABLOWITZ, M. J. & FOKAS, A. S. 2003 *Complex Variables: Introduction and Applications*. Cambridge University Press.
- ABRAMOWITZ, M. & STEGUN, I. A. 1964 *Handbook of mathematical functions*. New York: Dover Publications.
- ATASSI, H. M. 1984 The Sears problem for a lifting airfoil revisited - new results. *J. Fluid Mech.* **141**, 109–122.
- ATASSI, H. M., DUSEY, M. & DAVIS, C. M. 1993 Acoustic radiation from a thin airfoil in nonuniform subsonic flows. *AIAA Journal* **31** (1), 12–19.
- AYTON, L. J. 2016 Acoustic scattering by a finite rigid plate with a poroelastic extension. *Journal of Fluid Mechanics* **791**, 414–438.
- BADDOO, P. J., HAJIAN, R. & JAWORSKI, J. W. 2019 A Jacobi spectral collocation method for the steady aerodynamics of porous aerofoils. In *AIAA Aviation 2019 Forum*. Dallas, TX: Paper AIAA-2019-2959.
- BAUER, A. B. 1977 Impedance theory and measurements on porous acoustic liners. *Journal of Aircraft* **14** (8), 720–728.
- BIRD, H. J., OTOMO, S., RAMESH, K. K. & VIOLA, I. M. 2019 A geometrically non-linear

- time-domain unsteady lifting-line theory. In *AIAA Scitech 2019 Forum*. Dallas, TX: Paper AIAA-2019-1377.
- BIRD, R. B., STEWART, W. E. & LIGHTFOOT, E. N. 1960 *Transport Phenomena*. Wiley.
- BISPLINGHOFF, R. L., ASHLEY, H. & HALFMAN, R. L. 1996 *Aeroelasticity*. New York: Dover Publications.
- CORDES, U., KAMPERS, G., MEISSNER, T., TROPEA, C., PEINKE, J. & HÖLLING, M. 2017 Note on the limitations of the Theodorsen and Sears functions. *J. Fluid Mech.* **811**, R1.
- CORKERY, S. J., BABINSKY, H. & GRAHAM, W. R. 2019 Quantification of added-mass effects using particle image velocimetry data for a translating and rotating flat plate. *Journal of Fluid Mechanics* **870**, 492–518.
- DARWISH, M. A. 1999 Fredholm-Volterra integral equation with singular kernel. *Korean J. Comput. Appl. Math.* **6** (1), 163–174.
- DLMF 2019 *NIST Digital Library of Mathematical Functions*. <http://dlmf.nist.gov/>, Release 1.0.24 of 2019-09-15, f. W. J. Olver, A. B. Olde Daalhuis, D. W. Lozier, B. I. Schneider, R. F. Boisvert, C. W. Clark, B. R. Miller, B. V. Saunders, H. S. Cohl, and M. A. McClain, eds.
- ELDREDGE, J. D. 2010 A reconciliation of viscous and inviscid approaches to computing locomotion of deforming bodies. *Experimental Mechanics* **50**, 1349–1353.
- ERDOGAN, F. & GUPTA, G. D. 1972 On the numerical solution of singular integral equations. *Q. Appl. Math.* **29** (4), 525–534.
- ERDOGAN, F., GUPTA, G. D. & COOK, T. S. 1973 Numerical solution of singular integral equations. In *Methods of Analysis and Solutions of Crack Problems. Mechanics of Fracture* (ed. G. C. Sih), vol. 1, pp. 368–425. Dordrecht: Springer.
- ERGUN, S. 1952 Fluid flow through packed columns. *Chem. Eng. Prog.* **48** (2), 89–94.
- FFOWCS WILLIAMS, J. E. 1972 The acoustics of turbulence near sound-absorbent liners. *Journal of Fluid Mechanics* **51** (4), 737–749.
- FLORYAN, D., VAN BUREN, T., ROWLEY, C. W. & SMITS, A. J. 2017 Scaling the propulsive performance of heaving and pitching foils. *Journal of Fluid Mechanics* **822**, 386–397.
- GARRICK, I. E.. 1936 Propulsion of a flapping and oscillating airfoil. *NACA Report 567*.
- GEYER, T. & SARRADJ, E. 2014 Trailing edge noise of partially porous airfoils. In *20<sup>th</sup> AIAA/CEAS Aeroacoustics Conference*. Atlanta, GA: Paper AIAA-2014-3039.
- GEYER, T., SARRADJ, E. & FRITZSCHE, C. 2010 Measurement of the noise generation at the trailing edge of porous airfoils. *Experiments in Fluids* **48** (2), 291–308.
- GLEGG, S. & DEVENPORT, W. 2017 *Aeroacoustics of low Mach number flows: fundamentals, analysis, and measurement*. Academic Press.
- GOLDSTEIN, M. E. & ATASSI, H. 1976 A complete second-order theory for the unsteady flow about an airfoil due to a periodic gust. *Journal of Fluid Mechanics* **74** (4), 741–765.
- GRAHAM, J. M. R. 1970 Similarity rules for thin aerofoils in non-stationary subsonic flows. *Journal of Fluid Mechanics* **43** (4), 753–766.
- GROSJEAN, C. C. 1986 The weight functions, generating functions and miscellaneous properties of the sequences of orthogonal polynomials of the second kind associated with the Jacobi and the Gegenbauer polynomials. *Journal of Computational and Applied Mathematics* **16** (3), 259–307.
- HAJIAN, R. & JAWORSKI, J. W. 2017 The steady aerodynamics of aerofoils with porosity gradients. *Proceedings of the Royal Society A* **473**, 20170266.
- HAJIAN, R. & JAWORSKI, J. W. 2019 Noncirculatory fluid forces on panels with porosity gradients. *AIAA Journal* **57** (2), 870–875.
- HAJIAN, R., JAWORSKI, J. W. & GRACE, S. M. 2018 Acoustic emission from one-dimensional vibrating porous panels in a single-sided flow. In *AIAA/CEAS Aeroacoustics Conference*. Atlanta, GA: Paper AIAA-2018-2962.
- HANNA, Y. G. & SPEDDING, G. R. 2019 Aerodynamic performance improvements due to porosity in wings at moderate Re. In *AIAA Aviation 2019 Forum*. Dallas, TX: Paper AIAA-2019-3584.
- HOWE, M. S. 1979 On the theory of unsteady high Reynolds number flow through a circular aperture. *Proceedings of the Royal Society of London A* **366** (1725), 205–223.
- HOWE, M. S. 2002 *Theory of vortex sound*. United Kingdom: Cambridge University Press.



- IOSILEVSKII, G. 2011 Aerodynamics of permeable membrane wings. *European Journal of Mechanics B/Fluids* **30**, 534–542.
- IOSILEVSKII, G. 2013 Aerodynamics of permeable membrane wings. Part 2: Seepage drag. *European Journal of Mechanics B/Fluids* **39**, 32–41.
- JAWORSKI, J. W. 2012 Thrust and aerodynamic forces from an oscillating leading edge flap. *AIAA Journal* **50** (12), 2928–2931.
- JAWORSKI, J. W. & GORDNIER, R. E. 2012 High-order simulations of low Reynolds number membrane airfoils under prescribed motion. *Journal of Fluids and Structures* **31**, 49–66.
- JAWORSKI, J. W. & GORDNIER, R. E. 2015 Thrust augmentation of flapping airfoils in low Reynolds number flow using a flexible membrane. *Journal of Fluids and Structures* **52**, 199–209.
- JAWORSKI, J. W. & PEAKE, N. 2013 Aerodynamic noise from a poroelastic edge with implications for the silent flight of owls. *Journal of Fluid Mechanics* **723**, 456–479.
- JAWORSKI, J. W. & PEAKE, N. 2020 Aeroacoustics of silent owl flight. *Annual Review of Fluid Mechanics* **52**, 395–420.
- JORDAN, P. M. 2005 Growth and decay of acoustic acceleration waves in Darcy-type porous media. *Proceedings of the Royal Society of London A* **461** (2061), 2749–2766.
- KERSCHEN, E. J., TSAI, C. T. & MYERS, M. R. 1993 Influence of airfoil shape and incidence angle on high-frequency gust interaction noise. In *Unsteady Aerodynamics, Aeroacoustics, and Aeroelasticity of Turbomachines and Propellers*, pp. 765–782. Springer-Verlag.
- KISIL, A. & AYTON, L. J. 2018 Aerodynamic noise from rigid trailing edges with finite porous extensions. *Journal of Fluid Mechanics* **836**, 117–144.
- KRENK, S. 1975 On quadrature formulas for singular integral equations of the first and the second kind. *Q. Appl. Math.* **33** (3), 225–232.
- LEONARD, A. & ROSHKO, A. 2001 Aspects of flow-induced vibration. *Journal of Fluids and Structures* **15**, 415–425.
- LIFANOV, I. K., MATVEEV, A. F. & MOLYAKOV, I. M. 1992 Flow around permeable and thick airfoils and numerical solution of singular integral equations. *Russian Journal of Numerical Analysis and Mathematical Modelling* **7** (2), 109–144.
- LOEWY, R. G. 1957 A two-dimensional approximation to the unsteady aerodynamics of rotary wings. *Journal of the Aeronautical Sciences* **24** (2), 81–92.
- MOORE, M. N. J. 2014 Analytical results on the role of flexibility in flapping propulsion. *J. Fluid Mech.* **757**, 599–612.
- MOORE, M. N. J. 2015 Torsional spring is the optimal flexibility arrangement for thrust production of a flapping wing. *Phys. Fluids* **27** (9), 091701.
- MUSKHELISHVILI, N. I. 1946 *Singular integral equations*. Groningen: Noordhoff.
- NAYFEH, A. H., KAISER, J. E. & TELIONIS, D. P. 1975 Acoustics of aircraft engine-duct systems. *AIAA Journal* **13** (2), 130–153.
- NELSON, P. A. 1982 Noise generated by flow over perforated surfaces. *Journal of Sound and Vibration* **83** (1), 11–26.
- PETERS, D. A. 2008 Two-dimensional incompressible unsteady airfoil theory—an overview. *Journal of Fluids and Structures* **24** (3), 295–312.
- POLYANIN, A. 1998 *Handbook of Integral Equations*. CRC Press.
- RAMESH, K., GOPALARATHNAM, A., GRANLUND, K., OL, M. V. & EDWARDS, J. R. 2014 Discrete-vortex method with novel shedding criterion for unsteady aerofoil flows with intermittent leading-edge vortex shedding. *Journal of Fluid Mechanics* **751**, 500–538.
- RIENSTRA, S. W. 1992 A note on the Kutta condition in Glauert’s solution of the thin aerofoil problem. *Journal of Engineering Mathematics* **26** (1), 61–69.
- SCHWARZ, L. 1940 Berechnung der Druckverteilung einer harmonisch sich verformenden Tragfläche in ebener Strömung. *Luftfahrtforschung* **17**, 379–386.
- SCOTT, J. R. & ATASSI, H. M. 1993 High frequency gust interaction with single loaded airfoils in subsonic flows. In *Unsteady Aerodynamics, Aeroacoustics, and Aeroelasticity of Turbomachines and Propellers*, pp. 743–764. Springer-Verlag.
- SEARS, W. R. 1941 Some aspects of non-stationary airfoil theory and its practical application. *AIAA Journal* **8** (3), 104–108.
- SÖHNGEN, H. 1939 Die Lösungen der Integralgleichung und deren Anwendung in der Tragflügeltheorie. *Mathematische Zeitschrift* **45**, 245–264.

- SURESHBABU, A., RAMESH, K. & GOPALARATHNAM, A. 2019 Model reduction in discrete-vortex methods for unsteady airfoil flows. *AIAA Journal* pp. 1–14.
- SZEGO, G. 1939 *Orthogonal polynomials*. American Mathematical Society.
- TAHA, H. & REZAEI, A. S. 2019 Viscous extension of potential-flow unsteady aerodynamics: the lift frequency response problem. *J. Fluid Mech.* **868**, 141–175.
- THEODORSEN, T. 1935 General theory of aerodynamic instability and the mechanism of flutter. *NACA Report 496* .
- TREFETHEN, L. N. 2000 *Spectral Methods in MATLAB*. Society for Industrial and Applied Mathematics (SIAM, 3600 Market Street, Floor 6, Philadelphia, PA 19104).
- TZEZANA, G. A. & BREUER, K. S. 2019 Thrust, drag and wake structure in flapping compliant membrane wings. *J. Fluid Mech.* **862**, 871–888.
- WEGERT, E. 1990 An iterative method for solving nonlinear Riemann-Hilbert problems. *J. Comput. Appl. Math.* **29** (3), 311–327.
- WEGERT, E., WOLFERSDORF, L. V. & MEISTER, E. 1987 Plane potential flow past a cylinder with porous surface. *Math. Methods Appl. Sci.* **9** (1), 587–605.
- WEI, N. J., KISSING, J., WESTER, T. T. B., WEGT, S., SCHIFFMANN, K., JAKIRLIC, S., HÖLLING, M., PEINKE, J. & TROPEA, C. 2019 Insights into the periodic gust response of airfoils. *J. Fluid Mech.* **876**, 237–263.
- WEIDENFELD, M. & ARAD, E. 2018 Mitigating the sound of a flapping airfoil using optimal structural properties distributions. *J. Sound Vib.* **432**, 235–248.
- WEIDENFELD, M. & MANELA, A. 2016 On the attenuating effect of permeability on the low frequency sound of an airfoil. *Journal of Sound and Vibration* **375**, 275–288.
- WU, T. Y. T. 1961 Swimming of a waving plate. *J. Fluid Mech.* **10** (3), 321–344.
- YANG, Y., LI, M. & LIAO, H. 2019 Three-dimensional effects on the transfer function of a rectangular-section body in turbulent flow. *J. Fluid Mech.* **872**, 348–366.